

Entanglement distillation based on polarization and frequency hyperentanglement

Dan Xu,^{1,*} Changjia Chen,¹ Brian T. Kirby,^{2,3} and Li Qian^{1,†}

¹*Department of Electrical and Computer Engineering,
University of Toronto, Toronto, ON, M5S 3G4 Canada*

²*DEVCOM US Army Research Laboratory, Adelphi, MD 20783, USA*

³*Tulane University, New Orleans, LA 70118, USA*

(Dated: April 5, 2023)

Entanglement distillation has many applications in quantum information processing and is an important tool for improving the quality and efficiency of quantum communication, cryptography, computing, and simulation. We propose an entanglement distillation scheme using only one pair of polarization-frequency hyperentangled photons, which can be equivalently viewed as containing two pairs of entangled logical qubits: a pair of polarization-entangled qubits and a pair of frequency-entangled qubits. To perform the required CNOT operation between the two qubits we consider the use of a polarization-dependent frequency converter. Compared to past methods of entanglement distillation that relied on polarization and spatial-mode/energy-time degree of freedom, the utilization of frequency-encoded qubits offers an advantage in that it is immune to bit-flip errors when the channel is linear. After distillation, the fidelity of polarization entanglement can be significantly improved by sacrificing the frequency degree of freedom. Through simulation, we show that high fidelity gains, large yield, and high distillation rate can be achieved. Our distillation scheme is simple to implement with current technologies, compatible with existing telecommunication fiber networks, and is a promising approach for achieving efficient quantum communication.

I. INTRODUCTION

Distribution of entangled states between distant locations will be essential for the future large-scale realization of quantum communication schemes such as quantum teleportation [1], quantum dense coding [2], quantum cryptography [3], quantum digital signature [4, 5], coin-flipping [6] as well as quantum-enhanced metrological schemes [7] and quantum computation [8]. However, noise in the quantum channels and interactions with the environment are unavoidable, leading to decoherence and the degradation of entanglement.

To counteract such detrimental effects, entanglement distillation (ED), also referred to as entanglement purification, was introduced. The ED protocol was first proposed by Bennett et al. in 1996 and was further developed in both theory and experiment [9–14]. In the original (or two-copy) ED protocol, two imperfectly entangled pairs are consumed to generate, with some nonzero probability, a single entangled pair of a higher fidelity to a maximally entangled state. To perform ED, two different and independent entangled pairs are shared between remote users simultaneously. Once shared, the remote users conduct distillation by each performing a local CNOT operation between their portion of the two entangled states accompanied by the detection of one of the pairs which herald success or failure. The heralded results based on the detection of the target pairs will lead to a higher probability of retaining the desirable entangled states and discarding the noise states. Such distillation

processes can be repeated to obtain high-fidelity entangled states by sacrificing a large amount of low-fidelity pairs. Experimental implementations of such ED protocols, however, face the challenge of low efficiency and low distillation rates, as they are substantially limited by the low transmission probabilities of multiple photon pairs.

More recently, to overcome low efficiency, new ED protocols were proposed using only one copy of imperfect hyperentangled states [15, 16]. Hyperentanglement, the simultaneous and independent entanglement of quantum particles in multiple degrees of freedom (e.g. frequency, time-bin, polarization, orbital angular momentum), significantly expands the dimensionality of the Hilbert space of biphotons [17–19]. In practice, hyperentanglement can be naturally produced in certain spontaneous parametric downconversion (SPDC) processes. By constructing a “CNOT” gate between different degrees of freedom (DoFs), e.g., between polarization and spatial-mode or between polarization and energy-time DoFs, the entanglement in the latter DoF can be sacrificed to distill the polarization entanglement. Such hyperentanglement-based ED uses only one pair of photons to distill out a higher quality of entanglement in one DoF by sacrificing the other DoF, resulting in a dramatically improved efficiency. Though hyperentanglement-based ED is efficient, the process cannot be repeated indefinitely since, after one purification step, the entanglement in the other DoF is sacrificed. Therefore, it is desirable to obtain a significant improvement in fidelity in one step. The ED protocol in Ref. [15] using the energy-time DoF is more robust in in-field distribution than the spatial mode DoF used in Ref. [16], because the former does not need to transmit multiple spatial modes coherently over a long distance. On the other hand, the measurement of energy-time DoF requires modified Franson interferometers, which need to

* xudan.xu@utoronto.ca

† l.qian@utoronto.ca

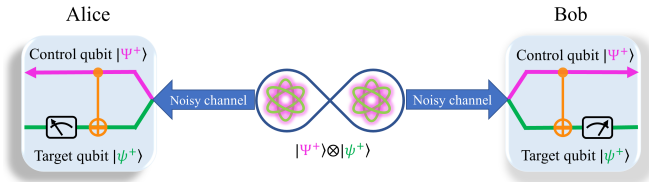


FIG. 1. A conceptual illustration of entanglement distillation protocol using polarization-frequency hyperentanglement. The hyperentangled state $|\Psi^+\rangle \otimes |\psi^+\rangle$ is first generated by an entanglement source and then distributed to Alice and Bob over two quantum channels. Alice and Bob apply a “CNOT” gate between two entangled subspaces encoded in the polarization (control qubit) and frequency (target qubit) degrees of freedom of a single photon pair. The successful distillation of the polarization entanglement is achieved after postselection based on the measurement results in the frequency DoF.

be stabilized at both remote sites, increasing the complexity of the distillation setup significantly.

Here we propose an ED protocol exploiting hyperentanglement in the polarization and frequency DoFs, which is both robust to channel degradation and eliminates the need for interferometric stability. Entanglement distillation relies on the “CNOT” gates with the polarization DoF as the control qubit and the frequency DoF as the target qubit. A conceptual diagram is shown in Fig. 1. We analyze our distillation scheme regarding fidelity, yield, and distillation rate. We compare it with the ED protocols using two copies [9], as well as using the polarization-energy-time (PET) [15] and the polarization-spatial mode (PSM) [16] hyperentanglement. Our entanglement distillation approach is highly efficient, robust, and easy to integrate into existing telecommunication fiber networks and can thus become a vital building block of future quantum internet.

II. PROPOSAL

Our proposed polarization entanglement distillation protocol uses only one pair of hyperentanglement in the polarization and frequency DoFs. We consider control and target implemented as polarization and frequency qubits, respectively. We denote the state of a horizontally polarized photon by $|H\rangle$ and the state of a vertically polarized photon by $|V\rangle$. As shown in Fig. 1, the hyperentangled photon source generates one pair of hyperentangled states which can be written as

$$|\phi\rangle = |\Psi^+\rangle_{ab} \otimes |\psi^+\rangle_{ab}. \quad (1)$$

$|\Psi^+\rangle_{ab}$ is the polarization Bell state

$$|\Psi^+\rangle_{ab} = \frac{1}{\sqrt{2}}(|H\rangle_a |V\rangle_b + |V\rangle_a |H\rangle_b), \quad (2)$$

and $|\psi^+\rangle_{ab}$ is the frequency Bell state

$$|\psi^+\rangle_{ab} = \frac{1}{\sqrt{2}}(|\omega_s\rangle_a |\omega_i\rangle_b + |\omega_i\rangle_a |\omega_s\rangle_b) \quad (3)$$

where ω_s, ω_i are the frequencies of the signal and idler photons, and the photons at Alice’s and Bob’s locations are denoted by a and b , respectively. The hyperentangled photons are distributed to Alice and Bob across a quantum channel. During distribution over a noisy channel, a phase flip (PF) error ($|\Psi^-\rangle_{ab}$) and a bit flip (BF) error ($|\Phi^+\rangle_{ab}$), as well as a bit-phase flip (BPF) error ($|\Phi^-\rangle_{ab}$), may be introduced to the polarization state. Due to the energy conservation of the SPDC process, the frequency Bell states could only be in $|\psi^+\rangle$ and $|\psi^-\rangle$. Additionally, assuming the channel is linear, no BF ($|\phi^+\rangle_{ab}$) or BPF error ($|\phi^-\rangle_{ab}$) can occur in frequency qubits. As we shall see later, the robustness in transmitting frequency qubits results in a drastic improvement in fidelity gain for the polarization qubits after distillation. For this reason, it is desirable to use frequency as an auxiliary DoF.

Following transmission over a noisy channel, the initial hyperentangled state becomes a mixed state as

$$\rho_{ab} = \rho_{ab}^p \otimes \rho_{ab}^f, \quad (4)$$

with

$$\rho_{ab}^p = F_p |\Psi^+\rangle_{ab} \langle \Psi^+| + A |\Psi^-\rangle_{ab} \langle \Psi^-| + B |\Phi^+\rangle_{ab} \langle \Phi^+| + C |\Phi^-\rangle_{ab} \langle \Phi^-| \quad (5)$$

and

$$\rho_{ab}^f = F_f |\psi^+\rangle_{ab} \langle \psi^+| + (1 - F_f) |\psi^-\rangle_{ab} \langle \psi^-|, \quad (6)$$

where F_p, A, B, C are the probabilities of polarization states $|\Psi^+\rangle, |\Psi^-\rangle, |\Phi^+\rangle, |\Phi^-\rangle$, respectively, and $F_p + A + B + C = 1$. $F_f, (1 - F_f)$ are the probabilities of frequency states $|\psi^+\rangle$ and $|\psi^-\rangle$, respectively. Table I lists all the error types in the polarization and frequency states, as well as their corresponding probabilities.

Our distillation protocol is based on a polarization-dependent frequency converter which is essentially a single-photon “CNOT” gate between the polarization and frequency DoFs. We start the explanation of our purification scheme by discussing an ideal, simplified example. Suppose that the two “CNOT” gates (frequency converters) utilized in this protocol on Alice’s and Bob’s sides are identical and their frequency conversion efficiency $\eta = 100\%$. The distillation protocol is composed of the following steps:

Step 1: Alice and Bob obtain their entangled photons from a prime source in a hyperentangled state described by Eq. (1).

Step 2: Alice and Bob perform a “CNOT” operation on their received photons. Depending on the polarization state (control qubit) of the photon, the frequency (target qubit) of the photon is either left unchanged or converted.

The logic table of the ‘‘CNOT’’ operation is

$$\begin{aligned}
|\omega_s\rangle|H\rangle &\Rightarrow |\omega_s\rangle|H\rangle, \\
|\omega_i\rangle|H\rangle &\Rightarrow |\omega_i\rangle|H\rangle, \\
|\omega_s\rangle|V\rangle &\Rightarrow |\omega_i\rangle|V\rangle, \\
|\omega_i\rangle|V\rangle &\Rightarrow |\omega_s\rangle|V\rangle.
\end{aligned} \tag{7}$$

i.e., the frequency mode is flipped only if the photon incident on the frequency converter is vertically polarized. In practice, this can be achieved through a polarization-dependent nonlinear frequency conversion process involving a strong classical pump. Temporal distinguishability introduced between the H and V polarizations can be later erased in a compensation step.

Step 3: After the ‘‘CNOT’’ operation, it becomes a new mixed state as listed in Table I. The frequency states paired with the $|\Psi^+\rangle_{ab}$ state and its PF error $|\Psi^-\rangle_{ab}$ in polarization DoF are transformed as

$$\begin{aligned}
|\Psi^+\rangle \otimes |\psi^+\rangle &\xrightarrow{\text{CNOT}} |\Psi^+\rangle \otimes |\phi^+\rangle, \\
|\Psi^+\rangle \otimes |\psi^-\rangle &\xrightarrow{\text{CNOT}} |\Psi^+\rangle \otimes |\phi^-\rangle, \\
|\Psi^-\rangle \otimes |\psi^+\rangle &\xrightarrow{\text{CNOT}} |\Psi^-\rangle \otimes |\phi^+\rangle, \\
|\Psi^-\rangle \otimes |\psi^-\rangle &\xrightarrow{\text{CNOT}} |\Psi^-\rangle \otimes |\phi^-\rangle.
\end{aligned} \tag{8}$$

The frequency state paired with the BF and BPF states in polarization DoF remains unchanged as $|\psi^+\rangle$ or $|\psi^-\rangle$.

Step 4: Alice and Bob’s postselection is based on the frequency qubit after performing the CNOT operation. The cases in which the photon pairs are in the frequency state $|\psi^\pm\rangle_{ab}$ are discarded in postselection. It’s worth noting that distinguishing between $|\psi^+\rangle_{ab}$ and $|\psi^-\rangle_{ab}$ states during measurement is unnecessary because both will be discarded. The cases in which the photon pairs are in the frequency state $|\phi^\pm\rangle_{ab}$ are kept in postselection. As shown in Table I, all BF and BPF errors in polarization can be identified and discarded.

By applying our distillation procedure, they can thus create a new ensemble

$$\rho_{ab}^p = F_p' |\Psi^+\rangle_{ab} \langle \Psi^+| + (1 - F_p') |\Psi^-\rangle_{ab} \langle \Psi^-| \tag{9}$$

with a larger fraction $F_p' > F_p$ of entangled pairs in the desired polarization state $|\Psi^+\rangle_{ab}$ than before the distillation. We now analyze them in more detail to show that our distillation scheme also works for various noise scenarios.

III. ANALYSIS

The success of the distillation protocol can be evaluated by comparing the noisy state ρ_{ab}^p and the distilled state ρ_{ab}^p with each other. For this purpose, we utilize the quantum state fidelity F to the $|\Psi^+\rangle_{ab}$ state before and after the distillation. Here we only consider phase-flip error ($\rho_{\text{err}}^f = (1 - F_f) |\psi^-\rangle_{ab} \langle \psi^-|$) to the frequency DoF

and the frequency state can be described by Eq. (6) with fidelity F_f . It does not reduce generality, as this is the only error possible in a linear channel. In regards to the polarization DoF, to comprehensively evaluate the efficiency of the protocol, we take into account all potential errors.

Scenario 1 (BF or BPF error only): we first introduce a BF error ($\rho_{\text{err}}^p = B |\Phi^+\rangle_{ab} \langle \Phi^+|$) to the polarization DoF, i.e. $B = 1 - F_p, A = C = 0$. After the ‘‘CNOT’’ operation and postselection, the polarization fidelity of the distilled state was $F_p' = 1$. We also examine the BPF error ($\rho_{\text{err}}^p = C |\Phi^-\rangle_{ab} \langle \Phi^-|$) as an additional error type, i.e. $C = 1 - F_p, A = B = 0$. We observe that this error shows the same fidelity characteristics $F_p' = 1$ as the BF error. Thus, in the case of only BF or only BPF error, or both ($\rho_{\text{err}}^p = B |\Phi^+\rangle_{ab} \langle \Phi^+| + C |\Phi^-\rangle_{ab} \langle \Phi^-|$, i.e. $A = 0$), the polarization fidelity of the distilled state will be dramatically improved, $F_p' = 1$. Theoretically, our distillation scheme can distill the polarization back to the ideal Bell state $\rho^p = |\Psi^+\rangle_{ab} \langle \Psi^+|$.

Scenario 2 (PF error only): if we add any proportion of PF error ($\rho_{\text{err}}^p = A |\Psi^-\rangle_{ab} \langle \Psi^-|$) to the polarization DoF, i.e. $A = 1 - F_p, B = C = 0$. After the ‘‘CNOT’’ operation and postselection, the polarization fidelity of the distilled state was $F_p' = F_p$. However, in the case of pure PF error, our distillation protocol is still feasible. We first convert PF errors to BF errors ($|\Psi^-\rangle_{ab} \rightarrow |\Phi^+\rangle_{ab}$) through the Hadamard operations and then complete entanglement distillation. The fidelity of polarization after distillation can still be $F_p' = 1$.

Scenario 3 (all errors together): Let’s consider that all types of errors together ($\rho_{\text{err}}^p = A |\Psi^-\rangle_{ab} \langle \Psi^-| + B |\Phi^+\rangle_{ab} \langle \Phi^+| + C |\Phi^-\rangle_{ab} \langle \Phi^-|$) are added to the polarization state. The presence of PF error in combination with BF and BPF errors cannot be separated through distillation, resulting in a reduction in fidelity gain after distillation. In such case, the polarization fidelity of the distilled state $F_p' = \frac{F_p}{F_p + A}$, which is still greater than F_p , indicates that our distillation scheme was still effective.

The theoretical analysis predicts that our distillation protocol can deal with various noise scenarios. We use the gain $G = F_p' - \max(F_p, F_f)$ as our figure of merit. We can see that the fidelity gain G is positive over all the regions $F_p \in [0, 1]$ & $F_f \in [0, 1]$ for **Scenario 1 (BF error only)** (as shown in Fig. 2). For example, the estimated theoretical fidelity gain after distillation is $G = 0.5$ for an initially mixed state with $F_p = F_f = 0.5$. This is much higher than the fidelity of the polarization or frequency state before distillation. In addition, we can obtain much higher positive gain in the low fidelity ranges, which shows that our distillation scheme is effective even in the high noise regions.

Another important figure of merit for distillation protocols is the yield, Y , defined as the number of distilled photon pairs divided by the total number of coincident photon pairs. For **Scenario 1 (BF error only)**, the yield Y increases linearly with the initial fidelity of the polarization state, $Y = F_p$, while it is independent of the

TABLE I. All the error types in the polarization and the frequency and their corresponding probabilities before and after distillation. The postselection is based on the frequency state: the photon pairs in the state $|\phi^\pm\rangle_{AB}$ will be kept and in the state $|\psi^\pm\rangle_{AB}$ will be discarded.

Initial state				After ‘‘CNOT’’			Postselection
Polarization	Probability	Frequency	Probability	Polarization	Frequency	Probability	Decision
$ \Psi^+\rangle$	F_p	$ \psi^+\rangle$	F_f	$ \Psi^+\rangle$	$ \phi^+\rangle$	$F_p F_f$	keep
		$ \psi^-\rangle$	$1 - F_f$		$ \phi^-\rangle$	$F_p(1 - F_f)$	keep
$ \Psi^-\rangle$ (PF error)	A	$ \psi^+\rangle$	F_f	$ \Psi^-\rangle$	$ \phi^+\rangle$	$A F_f$	keep
		$ \psi^-\rangle$	$1 - F_f$		$ \phi^-\rangle$	$A(1 - F_f)$	keep
$ \Phi^+\rangle$ (BF error)	B	$ \psi^+\rangle$	F_f	$ \Phi^+\rangle$	$ \psi^+\rangle$	$B F_f$	discard
		$ \psi^-\rangle$	$1 - F_f$		$ \Phi^-\rangle$	$B(1 - F_f)$	discard
$ \Phi^-\rangle$ (BPF error)	C	$ \psi^+\rangle$	F_f	$ \Phi^-\rangle$	$ \psi^+\rangle$	$C F_f$	discard
		$ \psi^-\rangle$	$1 - F_f$		$ \Phi^+\rangle$	$C(1 - F_f)$	discard

fidelity of the frequency state F_f (as shown in Fig. 2).

IV. COMPARISON WITH PSM AND PET HYPERENTANGLEMENT

In this section, we evaluate and contrast three distillation protocols that employ hyperentanglement. The first utilizes PET hyperentanglement [15], the second relies on PSM hyperentanglement [16], and the third is our work based on polarization-frequency hyperentanglement. We use fidelity gain and yield as metrics, and tabulate the results in Fig. 2. The protocols based on PET and PSM hyperentanglement obtain the same fidelity gain and yield in the range of $0.5 < F_p < 1$ & $0.5 < F_{e-t}$ or $F_s < 1$. Their polarization fidelity of the distilled state depends on the fidelities of the initial state in both DoFs. In contrast, our polarization-frequency distillation protocol will produce more gain across the entire range of possible input fidelities. We can even obtain a high positive gain in the low fidelity range $F_p, F_f < 0.5$.

Next, let us consider the distillation efficiency ξ , which consists of three parts: 1) the generation efficiency of the entangled source, 2) the transmission efficiency of the channel, and 3) the yield of the distillation protocol. Compared to the original (or two-copy) ED scheme, the hyperentanglement-based ED has much higher distillation efficiency. For typical experimental parameters (a mean number of photon pairs per pulse of $p = 0.001$ at a repetition of 76 MHz, a yield of $Y = 0.8$) and two 100 km fiber-based quantum channels, the PET single-copy distillation rate outperforms the two-copy scheme by 7 orders of magnitude [15]. Due to the higher loss of multi-mode fiber (MCF), the PSM single-copy distillation rate is 5 orders of magnitude higher than the two-copy scheme [16]. In our case, assuming frequency conversion efficiency $\eta = 100\%$, which is in principle theoret-

ically attainable, we can achieve a distillation rate similar to that of PET. However, in reality, the conversion efficiency is reduced due to coupling losses and component losses. We note that a recent experimental result has achieved a single-photon frequency conversion efficiency of approximately 50% [20]. In this case, the yield will be slightly lower, the distillation rate is still comparable with the PET protocol.

Moreover, our distillation scheme has great practical advantages. First, our polarization-frequency hyperentanglement source using an all-fiber configuration [21] could be very compact as compared to realizations using the spatial-mode DoF, which additionally requires modifications of the SPDC source [16]. Second, the long-distance distribution of polarization and spatial-mode hyperentanglement has the difficulty of maintaining coherence and phase stability between different paths. However, the polarization-frequency hyperentanglement is insensitive to decoherence as both $|\psi^+\rangle$ and $|\psi^-\rangle$ in frequency DoF can be used for distillation with equal effectiveness, so essentially the polarization fidelity F'_p of the distilled state is independent of frequency fidelity F_f and our distillation scheme works as long as the channel remains linear. Third, we can use standard telecommunication fibers to transmit polarization-frequency hyperentangled photons, instead of multi-core fibers for polarization-spatial-mode hyperentanglement, so the distillation scheme we introduced can easily be integrated into the existing classical and quantum communication network. Moreover, the frequency is much more robust during transmission in in-field implementations as compared to realizations using the spatial-mode DoF, resulting in much higher quality entanglement in polarization DoF after entanglement distillation. Fourth, frequency entanglement, the same as the energy-time entanglement, arises from the energy conservation in the SPDC process. However, the scheme using energy-time DoF requires two

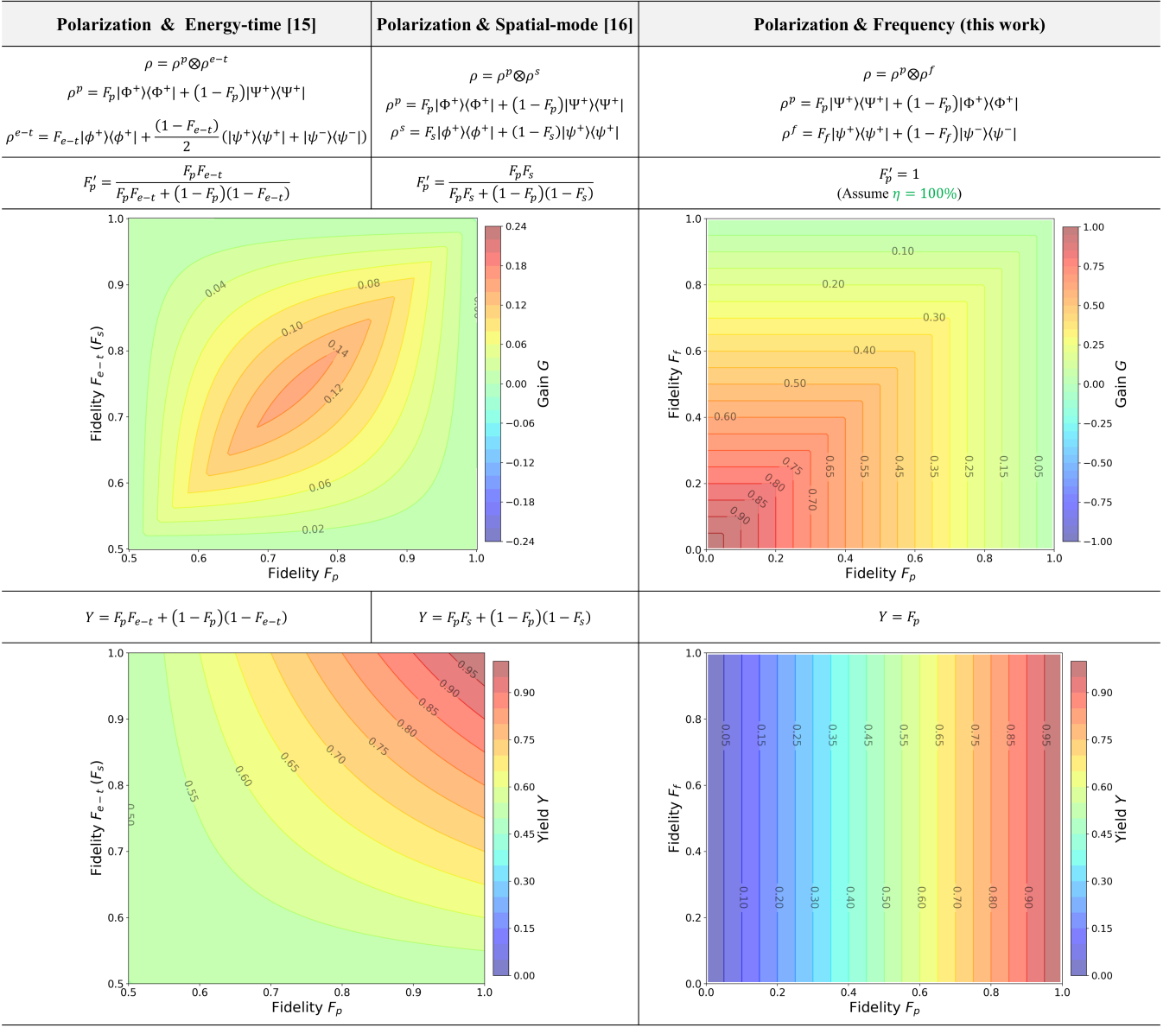


FIG. 2. Comparison of hyperentanglement-based distillation protocols: 1) polarization-energy-time (PET) hyperentanglement, 2) polarization-spatial-mode (PSM) hyperentanglement, 3) polarization-frequency hyperentanglement. For the sake of consistency with Ref. [15, 16], we only consider the polarization state $|\Psi^+\rangle$ with an admixed bit flip contribution $|\Phi^+\rangle$ and we define the gain $G = F_p' - \max(F_p, F_f)$. For the other DoFs, BF & BPF errors together are considered in PET protocol and only BF error is considered in PSM protocol, but we only consider PF error in frequency DoF because the channel is linear and BF & BPF errors for the frequency qubit cannot happen. For PET and PSM protocols, they obtain the same results and only $F_p \in [0.5, 1]$ & $F_{e-t}(F_s) \in [0.5, 1]$ are discussed because the fidelity gain G is positive only in these regions. For our protocol, with an assumption of $\eta = 100\%$, we can obtain a positive gain $G > 0$ in the whole range $F_p \in [0, 1]$ & $F_f \in [0, 1]$. The Yield $Y > 0.5$ when $F_p \in [0.5, 1]$ & $F_{e-t}(F_s) \in [0.5, 1]$ for PET (PSM) schemes. In contrast, our scheme has the Yield $Y = F_p$ independent of F_f . Due to the resilience of frequency to channel noise, our approach displays linear behavior, in contrast to the curved behavior exhibited by the other two schemes.

imbalanced Mach-Zehnder interferometers and needs active phase stabilization, which increases the complexity of the whole setup. Our scheme using frequency DoF is insensitive to channel length changes, so there is no need for recalibration. Fifth, in terms of ultimate transmission rates, the time delay between the arrival times of the en-

tangled photons limits the maximum bit rate that can be transmitted in polarization-energy-time hyperentanglement protocol. Polarization-frequency hyperentanglement, in contrast, has no such limitation and is therefore a promising approach for achieving high bit-rate communication.

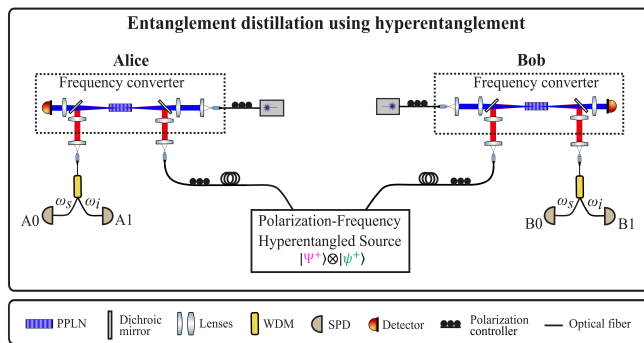


FIG. 3. Proposed experimental implementation for entanglement distillation in polarization and frequency. The hyperentangled state $|\Psi^+\rangle \otimes |\psi^+\rangle$ is first generated by the entanglement source where pairs of entangled photons are created in a periodically poled silica fiber (PPSF) [22]. Then the entangled photons are single-mode coupled and guided to Alice and Bob. After transmission through a noisy channel, entanglement distillation is performed. The entanglement distillation operation employs polarization-dependent frequency converters as the “CNOT” gates and converts the target qubit (frequency) according to the control qubit (polarization). The photons collected in paths A0, A1, B0, and B1 are detected and time tagged for post-selection.

V. PROPOSED IMPLEMENTATION

Hyperentanglement in polarization and frequency can be generated straightforwardly in fiber and nonlinear waveguides via nonlinear processes such as SPDC and spontaneous four-wave mixing (SFWM). As shown in Fig. 3, we propose to use a periodically poled silica fiber (PPSF) [21] to produce highly entangled photon pairs in these two DoFs. An effective second-order nonlinearity $\chi^{(2)}$ is artificially induced along the PPSF through the process of thermal poling, and the quasi-phase-matching allows for the direct generation of polarization-entangled photon pairs in PPSF at room temperature by exploiting type-II phase-matched SPDC [21, 22]. A pair of orthogonally polarized photons are generated by the down-conversion of a pump photon whose polarization is along the V axis of the PPSF. The photon pairs generated by the PPSF have a continuous spectrum with broad bandwidth and are naturally endowed with frequency entanglement due to energy conservation. The hyperentangled source generates one pair of photons in the hyperentangled state $|\Psi^+\rangle_{ab} \otimes |\psi^+\rangle_{ab}$. After the photons transmit to Alice and Bob over single-mode fibers, each photon’s polarization and frequency states become mixed, and the overall state is described by Eq. (4).

The frequency converters (FC) act as the single-photon “CNOT” gate. To be useful in our distillation scheme, FC must (i) allow frequency translation between the signal and idler photons, (ii) preserve the polarization entanglement of the original state, and (iii) must be highly efficient while not introducing additional unwanted “noise” photons. FC using three-wave mixing

(TWM) in second-order $\chi^{(2)}$ nonlinear optical media or four-wave mixing (FWM) in third-order $\chi^{(3)}$ nonlinear optical media can satisfy the above requirements [23–26]. For experimental implementation, we propose to realize the frequency conversion by difference frequency generation (DFG) in a periodically poled lithium niobate (PPLN) waveguide, though other nonlinear frequency conversion processes can be used as well. As shown in Fig. 3, the classical pump laser is combined with the signal/idler photons at a dichroic mirror (DM). Then, they are coupled into the type-0 quasi-phase-matched ($V \rightarrow V+V$) PPLN waveguide. If the polarization state of the signal/idler photon is horizontal, then it will not meet the phase-matching condition of the PPLN, and no frequency conversion occurs. If, on the other hand, the polarization state of the signal/idler photon is vertical, then the signal (or idler) photon will be frequency converted to the idler (or signal) frequency, i.e., $(|\omega_s\rangle|V\rangle \leftrightarrow |\omega_i\rangle|V\rangle)$. This polarization-dependent frequency conversion process is an equivalent “CNOT” operation between polarization qubit and frequency qubit.

After the “CNOT” operations at Alice and Bob, the photons are collected and separated by two wavelength splitters (WDMs), with signal frequency (ω_s) being directed to A0 and B0, and idler frequency (ω_i) being directed to A1 and B1. The successful distillation of the control qubit (polarization) is heralded by the measurement outcomes of the target qubit (frequency). In this case, either A0-B0 coincidences (i.e., both Alice and Bob detect ω_s) or A1-B1 coincidences (i.e. both detect ω_i) will be postselected, corresponding to frequency $|\phi^\pm\rangle_{ab}$ states. All other detection events will be discarded. Theoretically, a high conversion efficiency η close to unity can be expected for a frequency converter. Experimentally, however, the highest external device efficiency reported so far is 57% which is limited by the transmission through optical elements, fiber coupling, waveguide coupling, and spectral filtering [20]. Assume two FCs utilized in the scheme are identical and take the frequency conversion efficiency η into consideration, we can obtain a distilled state with the fidelity:

$$F'_p = \begin{cases} \frac{F_p}{F_p + (1-\eta)(1-F_p)}, & \text{(Scenario 1)} \\ \frac{F_p}{F_p + (1-\eta)(1-F_p)}, & \text{(Scenario 2)} \\ \frac{F_p}{F_p + A + (1-\eta)(B+C)}. & \text{(Scenario 3)} \end{cases} \quad (10)$$

Note that the definitions of these scenarios are provided in Section III. In the case of BF or BPF noise (**Scenario 1**) with a probability of $1 - F_p = 50\%$, the polarization fidelity after distillation became $F'_p = 0.7$ and the gain $G = 0.2$ (40% relative gain) can be obtained.

VI. CONCLUSION

In conclusion, we proposed an entanglement distillation protocol exploiting hyperentanglement in the polar-

ization and frequency DoFs. We analyzed different error types and characterized the post-distillation states in terms of the fidelity gain, yield, and distillation rate. These theoretical results are important for future experimental implementations. As our protocol shows, the fidelity gains are moderate in low-noise settings, while large gains are obtained in a high-noise regime where it really matters. We attribute this performance advantage to the relative robustness of the frequency DoF to common channel impairments as compared to PET and PSM schemes. This enables a significant increase in state quality in noise-dominated scenarios, recovering the potential for quantum communication applications in otherwise unattainable regimes. Compared to the PET and PSM approaches proposed in Ref[15, 16], our polarization-frequency scheme has certain significant practical advantages: a) Unlike in the case of PSM where multi-core fibers have to be used for transmitting multiple spatial modes, we can use standard telecommunication fibers to transmit polarization-frequency hyperentangled photons robustly; b) Unlike in the case of PET, our scheme does not involve interferometers and therefore no active phase stabilization is needed; c) Our scheme is insensitive to decoherence of frequency entanglement, making it a promising approach for practical applications; d) As

long as the channel is linear, frequency qubits do not suffer bit flip errors during transmission, resulting in high-quality entanglement in polarization degree of freedom after one-step distillation. Improved entanglement quality after entanglement distribution in a quantum network can have a number of benefits. For example, it can improve the security of the entanglement-based quantum key distribution (QKD) protocol, or the fidelity of the teleported state, result in higher quality and robustness of quantum error correction, or improve the accuracy and efficiency of quantum simulation. Overall, our proposed polarization-frequency hyperentanglement distillation protocol has the potential to unlock many previously inaccessible benefits in quantum communication, cryptography, computing, and simulation.

ACKNOWLEDGMENT

This research is supported by DEVCOM Army Research Laboratory Grant W911NF-20-2-0242 and by NSERC Alliance Grant (ALLRP 569583 EU-Canada joint project HyperSpace).

-
- [1] S. Pirandola, U. L. Andersen, L. Banchi, M. Berta, D. Bunandar, R. Colbeck, D. Englund, T. Gehring, C. Lupo, C. Ottaviani, J. L. Pereira, M. Razavi, J. S. Shaari, J. S. Shaari, M. Tomamichel, M. Tomamichel, V. C. Usenko, G. Vallone, P. Villoresi, and P. Wallden, *Adv. Opt. Photon.* **12**, 1012 (2020).
 - [2] Y. Guo, B.-H. Liu, C.-F. Li, and G.-C. Guo, *Adv. Quantum Technol.* **2**, 1900011 (2019).
 - [3] C. Portmann and R. Renner, *Rev. Mod. Phys.* **94**, 025008 (2022).
 - [4] C.-H. Zhang, X.-Y. Zhou, H.-J. Ding, C.-M. Zhang, G.-C. Guo, and Q. Wang, *Phys. Rev. Appl.* **10**, 034033 (2018).
 - [5] Y. Pelet, I. V. Puthoor, N. Venkatachalam, S. Wengerowsky, M. Lončarić, S. P. Neumann, B. Liu, Ž. Samec, M. Stipčević, R. Ursin, E. Andersson, J. G. Rarity, D. Aktas, and S. K. Joshi, *New J. Phys.* **24**, 093038 (2022).
 - [6] S. Neves, V. Yacoub, U. Chabaud, M. Bozzio, I. Kerendis, and E. Diamanti, “Experimental cheat-sensitive quantum weak coin flipping,” (2022), arXiv:2211.03472.
 - [7] L. Pezzè, A. Smerzi, M. K. Oberthaler, R. Schmied, and P. Treutlein, *Rev. Mod. Phys.* **90**, 035005 (2018).
 - [8] H.-S. Zhong, H. Wang, Y.-H. Deng, M.-C. Chen, L.-C. Peng, Y.-H. Luo, J. Qin, D. Wu, X. Ding, Y. Hu, P. Hu, X.-Y. Yang, W.-J. Zhang, H. Li, Y. Li, X. Jiang, L. Gan, G. Yang, L. You, Z. Wang, L. Li, N.-L. Liu, C.-Y. Lu, and J.-W. Pan, *Science* **370**, 1460 (2020).
 - [9] C. H. Bennett, G. Brassard, S. Popescu, B. Schumacher, J. A. Smolin, and W. K. Wootters, *Phys. Rev. Lett.* **76**, 722 (1996).
 - [10] J.-W. Pan, C. Simon, C. Brukner, and A. Zeilinger, *Nature* **410**, 1067 (2001).
 - [11] J.-W. Pan, S. Gasparoni, R. Ursin, G. Weihs, and A. Zeilinger, *Nature* **423**, 417 (2003).
 - [12] T. Yamamoto, M. Koashi, S. K. Ozdemir, and N. Imoto, *Nature* **421**, 343 (2003).
 - [13] P. Walther, K. J. Resch, C. Brukner, A. M. Steinberg, J.-W. Pan, and A. Zeilinger, *Phys. Rev. Lett.* **94**, 040504 (2005).
 - [14] L.-K. Chen, H.-L. Yong, P. Xu, X.-C. Yao, T. Xiang, Z.-D. Li, C. Liu, H. Lu, N.-L. Liu, L. Li, T. Yang, C.-Z. Peng, B. Zhao, Y.-A. Chen, and J.-W. Pan, *Nat. Photon.* **11**, 695 (2017).
 - [15] S. Ecker, P. Sohr, L. Bulla, M. Huber, M. Bohmann, and R. Ursin, *Phys. Rev. Lett.* **127**, 040506 (2021).
 - [16] X.-M. Hu, C.-X. Huang, Y.-B. Sheng, L. Zhou, B.-H. Liu, Y. Guo, C. Zhang, W.-B. Xing, Y.-F. Huang, C.-F. Li, and G.-C. Guo, *Phys. Rev. Lett.* **126**, 010503 (2021).
 - [17] J. T. Barreiro, N. K. Langford, N. A. Peters, and P. G. Kwiat, *Phys. Rev. Lett.* **95**, 260501 (2005).
 - [18] M. Barbieri, C. Cinelli, P. Mataloni, and F. De Martini, *Phys. Rev. A* **72**, 052110 (2005).
 - [19] M. Erhard, M. Krenn, and A. Zeilinger, *Nat. Rev. Phys.* **2**, 365 (2020).
 - [20] T. van Leent, M. Bock, R. Garthoff, K. Redeker, W. Zhang, T. Bauer, W. Rosenfeld, C. Becher, and H. Weinfurter, *Phys. Rev. Lett.* **124**, 010510 (2020).
 - [21] E. Y. Zhu, Z. Tang, L. Qian, L. G. Helt, M. Liscidini, J. E. Sipe, C. Corbari, A. Canagasabey, M. Ibsen, and P. G. Kazansky, *Phys. Rev. Lett.* **108**, 213902 (2012).
 - [22] C. Chen, E. Y. Zhu, A. Riazi, A. V. Gladyshev, C. Corbari, M. Ibsen, P. G. Kazansky, and L. Qian, *Opt. Ex-*

- press **25**, 22667 (2017).
- [23] H. J. McGuinness, M. G. Raymer, C. J. McKinstrie, and S. Radic, *Phys. Rev. Lett.* **105**, 093604 (2010).
- [24] J. S. Pelc, L. Ma, C. R. Phillips, Q. Zhang, C. Langrock, O. Slattery, X. Tang, and M. M. Fejer, *Opt. Express* **19**, 21445 (2011).
- [25] S. Ramelow, A. Fedrizzi, A. Poppe, N. K. Langford, and A. Zeilinger, *Phys. Rev. A* **85**, 013845 (2012).
- [26] M. Bock, P. Eich, S. Kucera, M. Kreis, A. Lenhard, C. Becher, and J. Eschner, *Nat. Commun.* **9**, 1998 (2018).